N-tert-butyloxycarbonyl-Phe-Leu-Phe-Leu-Phe (BOC2) inhibits the angiogenic activity of heparin-binding growth factors.

**_N_-tert-butyloxycarbonyl-Phe-Leu-Phe-Leu-Phe (BOC2) inhibits the angiogenic activity of heparin-binding growth factors.**

Imtiaz M. Nawaz[1], Paola Chiodelli[1], Sara Rezzola[1], Giuseppe Paganini[1], Michela Corsini[1], Alessio Lodola[2], Alessio Di Ianni[2], Marco Mor[2] and Marco Presta[1]

[1] Department of Molecular and Translational Medicine, University of Brescia, Italy

[2] Department of Food and Drug, University of Parma, Italy

Correspondence to: Marco Presta (email: marco.presta@unibs.it; phone: +39-030-3717311)

**Acknowledgments**

The authors wish to thank S. Matarazzo for technical support. This work was supported in part by Associazione Italiana per la Ricerca sul Cancro (IG AIRC grant n° 18493) to M.P.; S.R. was supported by an AIRC fellowship.

## Abstract

The peptides N-tert-butyloxycarbonyl-Phe-Leu-Phe-Leu-Phe (BOC2) and BOC-Met-Leu-Phe (BOC1) are widely used antagonists of formyl peptide receptors (FPRs), BOC2 acting as a FPR1/FPR2 antagonist whereas BOC1 inhibits FPR1 only. Extensive investigations have been performed by using these FPR antagonists as a tool to assess the role of FPRs in physiological and pathological conditions. Based on previous observations from our laboratory, we assessed the possibility that BOC2 may exert also a direct inhibitory effect on the angiogenic activity of vascular endothelial growth factor-A (VEGF-A). Our data demonstrate that BOC2, but not BOC1, inhibits the angiogenic activity of heparin-binding VEGF-$A_{165}$ with no effect on the activity of the non-heparin-binding VEGF-$A_{121}$ isoform. Endothelial cell-based bioassays, surface plasmon resonance analysis and computer modeling indicate that BOC2 may interact with the heparin-binding domain of VEGF-$A_{165}$, thus competing for heparin interaction and preventing the binding of VEGF-$A_{165}$ to tyrosine kinase receptor VEGFR2, its phosphorylation and downstream signaling. In addition, BOC2 inhibits the interaction of a variety of heparin-binding angiogenic growth factors with heparin, including fibroblast growth factor 2 (FGF2) whose angiogenic activity is blocked by the compound. Accordingly, BOC2 suppresses the angiogenic potential of human tumor cell lines that co-express VEGF-A and FGF2. Thus, BOC2 appears to act as a novel multi-heparin-binding growth factor antagonist. These findings set the basis for the design of novel multi-target angiogenesis inhibitors and caution about the interpretation of FPR-focusing experimental data obtained with this compound.

## Keywords

Angiogenesis, BOC2, FGF2, Heparin binding, VEGF

## Electronic supplementary material

The online version of this article contains supplementary material, which is available to authorized users.

## Introduction

Angiogenesis is a process by which new vascular networks develop from preexisting vessels. It plays a pivotal role during embryonic development, wound healing, and tissue regeneration [1]. Uncontrolled angiogenesis occurs in several pathologies, including diabetic retinopathy [2], arthritis [3], immune disorders [4] and cancer [5].

Angiogenesis is regulated by the balance between negative and positive regulators that eventually will initiate the cascade of signal transduction pathways to promote endothelial cell migration, proliferation and vessel maturation [6]. Suppression of any of these steps would inhibit the formation of new vessels and will ameliorate abnormal neovascularization [7].

Various angiogenic growth factors have been identified that activate cognate signaling tyrosine kinase (TK) high-affinity receptors expressed by endothelial cells and share the capacity to interact with heparan sulfate proteoglycans (HSPGs) that act as low-affinity, high capacity co-receptors (see [8] for a review). They include, among others, members of the vascular endothelial growth factor (VEGF) and fibroblast growth factor (FGF) families, their prototypic members being represented by VEGF-$A_{165}$ and FGF2 that activate the endothelial pro-angiogenic TK receptors VEGFR2 and FGFR1, respectively [9,10].

The interaction of heparin-binding growth factors with HSPGs present on the cell surface and extracellular matrix contributes to their binding to cognate TK receptors, leading to the formation of bioactive HSPG/growth factor/TK receptor ternary complexes [11,12]. In addition, HSPG interaction stabilizes the growth factor in an active conformation, prevents its degradation, and greatly enhances the angiogenic response in endothelial cells [13,14].

The peptides N-tert-butyloxycarbonyl-Phe-Leu-Phe-Leu-Phe (BOC-FLFLF in single letter code, BOC2) and BOC-Met-Leu-Phe (BOC-MLF, BOC1) are widely used as antagonists of formyl peptide receptors (FPRs) [15]. FPRs are G protein-coupled receptors implicated in the regulation of innate immune responses, inflammation, tissue repair and angiogenesis [16]. Three FPRs have been identified in humans (FPR1–FPR3), BOC2 acting as a FPR1/FPR2 antagonist whereas BOC1 inhibits FPR1 only. Extensive investigations have been performed by using FPR antagonists as a tool to assess the role of FPRs in physiological and pathological conditions (see for instance [15,17] and references therein).

Recent findings from our laboratory had shown that BOC2, but not BOC1, is able to inhibit the angiogenic response exerted by the vitreous humor obtained after *pars plana* vitrectomy from

patients affected by proliferative diabetic retinopathy (PDR), thus suggesting a possible involvement of FPRs in this disease [18]. However, a variety of heparin-binding cytokines, chemokines and angiogenic growth factors are present in significant amounts in PDR vitreous, including VEGF-A [19-21]. Indeed, anti-angiogenic agents designed to block the activity of VEGF are widely used in PDR therapy [22] and pan-heparin-binding growth factor antagonists exert a significant inhibitory activity on angiogenic responses induced by heparin-binding VEGF-$A_{165}$ and PDR vitreous in pre-clinical settings [12]. Altogether, these observations prompted us to assess the possibility that BOC2 may exert a direct inhibitory effect on VEGF-A activity.

Here, our data demonstrate that BOC2, but not BOC1, inhibits the angiogenic activity of heparin-binding VEGF-$A_{165}$ with no effect on the activity of the non-heparin-binding VEGF-$A_{121}$ isoform. Accordingly, experimental evidences indicate that BOC2 may interact with the heparin-binding domain of VEGF-$A_{165}$, thus competing for heparin/HSPG interaction and preventing the binding of VEGF-$A_{165}$ to VEGFR2, its phosphorylation and downstream signaling. In addition, BOC2 inhibits the interaction of a variety of heparin-binding angiogenic growth factors with heparin, including FGF2 whose angiogenic activity is blocked by the compound. Accordingly, BOC2 suppresses the angiogenic potential of human tumor cell lines that co-express VEGF-A and FGF2.

In conclusion, BOC2 appears to act as a novel multi-heparin-binding growth factor antagonist. These findings set the basis for the design of novel multi-target angiogenesis inhibitors and caution about the interpretation of FPR-focusing experimental data obtained with this compound.

## Materials and Methods

### Reagents

BOC2 was from Phoenix Pharmaceuticals Inc. (Burlingame, CA); BOC1, BOC-F-OH, porcine gelatin, porcine heparin, endothelial cell growth factor and anti-α-tubulin were from Sigma-Aldrich (St. Louis, MO); M199, DMEM, RPMI 1640 media and FCS were from Gibco Life Technologies (Grand Island, NY); 1-phenyl-2-thiourea and tricaine were from Sigma-Aldrich (Saint Louis, MO); VEGF-$A_{165}$ and VEGF-$A_{121}$ were kindly provided by K. Ballmer-Hofer (PSI, Villigen, Switzerland); FGF2 was from Tecnogen (Caserta, Italy); hepatocyte growth factor (HGF), platelet-derived growth factor-B (PDGF-B) and recombinant human sFGFR1(IIIc)/Fc chimera (sFGFR1) were from ReliaTech (Wolfenbüttel, Germany); high mobility group box 1 (HMGB1) was from ProSpec (Rehovot, Israel); placental growth factor 2 (PlGF2) was kindly provided by S. De Falco (University of Naples, Italy); connective tissue growth factor (CTGF) and stromal cell-derived factor 1 (SDF1; CXCL12) were from PeproTech (Rock Hill, NJ); recombinant human VEGFR2-Fc

chimera protein (sVEGFR2) was from R&D system (Minneapolis, MN); TRIzol reagent and murine leukemia virus reverse transcriptase were from Invitrogen (Carlsbad, CA); anti-pVEGFR2, anti-pAKT and anti-pERK$_{1/2}$ antibodies were from Cell Signaling Technology (Beverly, MA); anti-FGFR1, anti-Focal Adhesion Kinase (FAK) and anti-total-ERK$_2$ were from Santa Cruz Biotechnology (Santa Cruz, CA).

**Cell cultures**

Human umbilical vein endothelial cells (HUVECs) were isolated from umbilical cords and used at early (I–IV) passages. Cells were grown on culture plate coated with porcine gelatin in M199 medium supplemented with 20% FCS, endothelial cell growth factor (10 μg/mL), and porcine heparin (100 μg/mL).

FGFR1-overexpressing fetal bovine aortic endothelial GM7373-flg cells [23] and human melanoma A2058 cells (provided by R. Giavazzi, Istituto Ricerche Farmacologiche Mario Negri, Milano, Italy), were grown in DMEM medium supplemented with 10% FCS. Human prostate cancer DU145 cells were obtained from ATCC repository and cultured in RPMI plus 10% FCS.

All cells were maintained in a humidified 5% $CO_2$ incubator at 37°C, with medium replaced every 2-3 days until cells reached confluency. Cells were maintained at low passage, returning to original frozen stocks every 3 to 4 months, and tested regularly for *Mycoplasma* negativity.

**Western blot analysis**

Cells were collected and washed in cold PBS and homogenized in RIPA buffer containing 1% Triton-X100, 0.1% BriJ, 1 mM sodium orthovanadate and protease inhibitors cocktail. The cell lysate was centrifuged and the supernatant was collected. Aliquots of each sample containing equal amounts of protein (20-50 μg) were subjected to SDS-PAGE. Gels were transblotted onto PVDF membrane and blots were blocked with 1% skim milk for 1 h at room temperature. Blotting analysis was performed with anti-pVEGFR2, anti-pFGFR1, anti-pAKT and anti-pERK$_{1/2}$ antibodies (1:1,000). After treating the membranes with appropriate secondary horseradish peroxidase-labeled secondary antibody (1:5,000), blots were developed with enhanced chemiluminescence reagent (Bio-rad Laboratories, Inc. Hercules, CA). Images were acquired (ChemiDoc Touch; Bio-Rad Laboratories, Inc.) and band intensity was evaluated (Image Lab 3.0 software; Bio-Rad Laboratories, Inc.). Data were normalized to the levels of FAK, α-tubulin or total ERK$_2$, as appropriate. After statistical analysis, data from independent set of experiments were plotted and averaged on the same graph.

**Endothelial cell proliferation assays**

HUVECs were seeded at $17x10^3$ cells/cm$^2$ and serum-starved overnight. Then, cells were stimulated with 30 ng/mL VEGF-$A_{165}$ and increasing concentrations of BOC2, BOC1 or BOC-F-OH in the presence of 2.5% FCS. FGFR1-overexpressing endothelial GM7373-flg cells [23] were seeded at $15x10^3$ cells/cm$^2$ and treated with 30 ng/mL of FGF2 and increasing concentrations of BOC2 in the presence of 1.25% FCS. After 48 h, cells were counted with a MACSQuant cytofluorimeter and cell proliferation was expressed as percentage of growth factor activity in the absence of any competitor.

**HUVEC sprouting assay**

HUVEC aggregates (800 cells/spheroid) were embedded in fibrin gel [18] and stimulated with VEGF-$A_{165}$, VEGF-$A_{121}$ or FGF2 and increasing concentrations of BOC2, BOC1 or BOC-F-OH. Sprouts were counted after 24 h and data were expressed as percentage of growth factor activity in the absence of any competitor.

**VEGF-$A_{165}$-mediated cell-cell adhesion assay**

This assay was performed as described [12]. Briefly, GAG-deficient A745 CHO cells were transfected with pCDNA3 harboring the human VEGFR2 extracellular domain (ECD) conjugated with yellow fluorescent protein (YFP) to generate stable ECD-VEGFR2-YFP A745 CHO cell transfectants. CHO-K1 cells expressing HSPGs and devoid of VEGFR2 was seeded in 24-well plates at $5x10^4$ cells/cm$^2$. After 24 h, ECD-VEGFR2-YFP cells ($5x10^4$ cells/cm$^2$) were added to CHO-K1 monolayers in the presence of VEGF-$A_{165}$ and increasing concentrations of BOC2. After 2 h at 4°C, ECD-VEGFR2-YFP cells bound to the CHO-K1 monolayer were photographed and counted.

**Surface plasmon resonance (SPR) analysis**

Biotinylated heparin was immobilized onto a BIAcore SA sensorchip (GE-Healthcare, WI) containing pre-immobilized streptavidin whereas sVEGFR2 and sFGFR1 were immobilized on activated CM5 sensorchips [12]. For competition experiments, VEGF or FGF2 (100 nM) *plus* increasing concentrations of BOC2 or BOC1 were injected over heparin, sVEGFR2 or sFGFR1 surfaces and bound analyte was measured [resonance units (RU)] at the end of injection. For

evaluation of BOC2/heparin-binding growth factor interaction, proteins were injected over the heparin surface in the presence of increasing BOC2 concentrations.

**Zebrafish yolk membrane (ZFYM) angiogenesis assay**

Zebrafish (*Danio rerio*) adults (AB strain) were maintained at 28°C on a 14 h light/10 h dark cycle under standard laboratory conditions. Embryos were incubated in fish water (0.1 g/L sodium bicarbonate; 0.19 g/L calcium sulphate; 0.1 g/L Crystal Sea) at 28°C and maintained in 0.003% 1-phenyl-2-thiourea starting from 24 hours post-fertilization (hpf) to prevent pigmentation. Zebrafish embryos were staged as described [24] and anesthetized with 0.016% tricaine. At 48 hpf, 40 ng/embryo of VEGF-$A_{165}$ were injected in the perivitelline space of zebrafish embryos in the proximity of developing subintestinal vein vessels (SIVs) using an InjectMan IN2 microinjector (Eppendorf) equipped with FemtoJet [25,26]. After 2 h, increasing concentrations of BOC2 were injected in the blood stream of treated embryos and the angiogenic response from the SIV basket, characterized by the ectopic growth of newly formed, alkaline phosphatase-positive blood vessels, was quantified at 72 hpf as described [27]. Briefly, embryos were fixed in 4% paraformaldehyde for 2 h at room temperature, dehydrated in methanol and stained with NBT/BCIP (Sigma) for endogenous alkaline phosphatase activity. Embryos were mounted in agarose-coated Petri dishes and photographed under a Leica MZ16 F stereomicroscope equipped with a QI ClicK Mono Uncooled Camera and Qcapture Pro software.

**Chick Embryo Chorioallantoic Membrane (CAM) Assay**

Alginate beads (4 µL) containing $2x10^4$ A2058 or DU145 cells added or not with 60 µM BOC2 were placed on the top of the CAM of fertilized white Leghorn chicken eggs at day 11 of incubation (7 eggs per experimental group) [28]. After 3 days, blood vessels converging toward the implant were counted under a stereomicroscope (STEMI-SR, x2/0.12; Zeiss) at x5 magnification.

**Semi-quantitative real-time PCR**

Steady-state transcription levels of *VEGF-A* and *FGF2* genes were evaluated in A2058 and DU145 cell lines by semi-quantitative real-time PCR (RT-PCR). Briefly, total RNA was extracted using TRIzol reagent accordingly to manufacturer's instructions (Invitrogen, Carlsbad, CA) and 2 µg of total RNA were retro-transcribed with MMLV reverse transcriptase (Invitrogen, Carlsbad, CA) using random hexaprimers in a final 20 µL volume. Then, 1/10th of the reaction was analyzed by semi-quantitative RT-PCR using the following primers:

*Human VEGF-A*: 5'-TGGATGTCTATCAGCGCAGCT-3' (forward); 5'-TGTTTTTGCAGGAACATTTACAC-3' (reverse);

*Human FGF2*: 5'-TGTGTCTATCAAAGGAGTGTG -3' (forward); 5'-CCGTAACACATTTAGAAGCCA -3' (reverse);

*Human GAPDH*: 5'-GAAGGTCGGAGTCAACGGATT-3' (forward); 5'-TGACGGTGCCATGGAATTTG-3' (reverse).

**Molecular modeling of BOC2/VEGF-HBD interaction**

*Induced-fit docking*: The structure of BOC2 was built with Maestro 10.5 (*Maestro*, version 10.5; Schrödinger, LLC: New York, 2016) and its geometry optimized with OPLS3 force field [29] in continuum solvent (GB/SA, water) to an energy gradient of 0.05 kcal $mol^{-1}$ $Å^{-2}$. The structure of the heparin-binding domain of VEGF-$A_{165}$ (VEGF-HBD) was taken from its X-ray complex with neuropilin-1 (4DEQ.pdb) [30]. VEGF-HBD was prepared for docking simulations using the protein preparation tools implemented in Maestro 10.5. The procedure included: *i.* addition of hydrogen atoms; *ii*. assignment of the protonation state of titratable amino acids at physiological pH; *iii.* geometric optimization of the whole system to a RMSD value of 0.3 Å. The prepared VEGF-HBD structure was used to perform docking simulations using the induced-fit protocol implemented in the Schrodinger package [31]. The docking grid was centered in a region of VEGF-HBD delimited by Arg13, Arg14, Lys15, Lys30, Arg35, Arg46 and Arg49, using enclosing and bounding boxes of 20 and 14 Å on each side, respectively. Among the five top-scoring poses, the BOC2 peptide took contacts with some of key basic residues (*i.e.* Arg14, Arg35, Arg39, Arg49) known to be recognized by the heparan sulfate [32] only in two of them. These two BOC2/VEGF-HBD complexes were submitted to energy minimization with OPLS3 force field in continuum solvent (GB/SA, water) to an energy gradient of 0.05 kcal $mol^{-1}$ $Å^{-2}$ and then to MD simulations.

*Molecular dynamics (MD) simulations:* MD simulations of energy-minimized BOC2/VEGF-HBD complexes were performed in explicit solvent. Desmond 4.5 (*Desmond Molecular Dynamics System*, version 4.5; D. E. Shaw Research: New York, 2016; *Maestro−Desmond Interoper-ability Tools*, version 4.5; Schrödinger: New York, 2016) was used to build the solvated systems, applying the TIP3P model for water and ensuring that the solute molecules were placed at least 20 Å far from their neighboring periodic images. The systems were then submitted to MD simulations performed in the NPT ensemble at 300 K and 1 atm, applying the Langevin coupling scheme [33]. Long-range electrostatic interactions were calculated applying the smooth particle mesh Ewald method [34] while short-range electrostatic and van der Waals interactions were cut off at 9 Å. The M-SHAKE

algorithm was used to constraint all bond lengths to hydrogens and a RESPA integrator was applied to schedule the calculation of short-range nonbonded interactions and long-range electrostatic interactions every 2 and 6 fs, respectively. During the simulations, restraints of 1 kcal $mol^{-1}$ were applied on the C alpha of the secondary structures of VEGF-HBD whereas the structure of BOC2 was left unrestrained.

### Statistical analysis

Statistical analysis was performed with GraphPad Prism 6 (San Diego, CA, USA) using one-way ANOVA followed by Bonferroni multiple comparison post-test or Student's *t*-test. The data are expressed as mean ± SEM and $P$ values < 0.05 were considered statistically significant.

## Results

### BOC2 inhibits the angiogenic activity of VEGF-$A_{165}$

In a first set of experiments, BOC2, BOC1 and BOC-F-OH (Supplementary Fig. S1) were assessed for their capacity to affect the activity of VEGF-$A_{165}$ in HUVECs. As shown in Fig. 1a-d, BOC2 inhibits VEGF-induced VEGFR2 phosphorylation and activation of the downstream secondary signaling mediators $EKR_{1/2}$ and AKT in HUVECs in a dose-dependent manner. No significant inhibition was exerted by BOC1 and BOC-F-OH, thus confirming the specificity of the effect (Fig. 1e,f).

In keeping with its ability to hamper VEGFR2 activation, BOC2 prevents VEGF-$A_{165}$-mediated HUVEC proliferation and sprouting of HUVEC spheroids embedded in a 3D fibrin gel (Fig. 1g-i). Again, no inhibitory effect was exerted by BOC1 or BOC-F-OH when tested under the same experimental conditions.

Next, the capacity of BOC2 to affect the angiogenic activity of VEGF-$A_{165}$ was assessed *in vivo* in zebrafish yolk membrane (ZFYM) angiogenesis assay [25,26]. To this aim, 40 ng/embryo of VEGF-$A_{165}$ were injected in the perivitelline space of zebrafish embryos in the proximity of developing subintestinal vessels (SIVs) at 48 hpf [25]. After 2 h, increasing concentrations of BOC2 were injected in the blood stream of treated embryos and the angiogenic response from the SIV basket, characterized by the ectopic growth of alkaline phosphatase-positive neovessels, was quantified at 72 hpf. As shown in Fig. 1j,k, BOC2 causes a dose-dependent inhibition of VEGF-$A_{165}$-induced SIV sprouting, with a maximal effect at the dose of 10 pmoles/embryo. Notably, no effect was exerted by BOC2 on the physiological formation of the SIV basket in PBS-treated embryos.

Together, these data demonstrate that BOC2 is able to abrogate VEGF-$A_{165}$ activity in endothelial cells *in vitro* and *in vivo*.

**BOC2 inhibits the formation of HSPG/VEGF-$A_{165}$/VEGFR2 ternary complexes**

HSPGs mediate the binding of VEGF-$A_{165}$ to its signaling receptor VEGFR2, leading to the formation of bioactive HSPG/VEGF-$A_{165}$/VEGFR2 ternary complexes [8]. To assess whether the anti-VEGF activity of BOC2 was due to its capacity to affect the formation of this bioactive complex, we used a cell-cell adhesion assay in which VEGF-$A_{165}$ mediates cell-cell adhesion events due to its simultaneous interaction with VEGFR2 and HSPGs expressed *in trans* on neighboring cells. In this assay, VEGF-$A_{165}$ allows the adhesion of HSPG-deficient CHO cell mutants overexpressing the extracellular domain of VEGFR2 (ECD-VEGFR2-YFP A745 CHO cells) when seeded on the top of a monolayer of HSPG-bearing CHO-K1 cells [12]. As shown in Fig. 2a, BOC2 prevents the adhesion of VEGFR2 transfectants to the HSPG-bearing cell monolayer, thus indicating its ability to prevent the formation of HSPG/VEGF-$A_{165}$/VEGFR2 ternary complexes.

To assess whether this activity was due to the ability of BOC2 to affect VEGF-$A_{165}$/VEGFR2 and/or VEGF-$A_{165}$/HSPG binary interactions, the compound was investigated by SPR analysis for its capacity to prevent the binding of VEGF-$A_{165}$ to heparin or sVEGFR2 immobilized to BIAcore sensor chips. In the absence of any competitor, the binding of VEGF-$A_{165}$ to immobilized sVEGFR2 or immobilized heparin occurs with $K_d$ values equal to 3.0 nM [35] and 100 nM [36], respectively. In keeping with its capacity to hamper the formation of bioactive HSPG/VEGF/VEGFR2 tertiary complexes, BOC2 inhibits with a similar potency the binding of VEGF-$A_{165}$ to immobilized sVEGFR2 and heparin, whereas BOC1 was ineffective (Fig. 2b,c).

**BOC2 interacts with the heparin-binding domain of VEGF-$A_{165}$**

VEGF-$A_{165}$ contains a heparin-binding domain (VEGF-HBD) absent in the VEGF-$A_{121}$ isoform [9]. The capacity of BOC2 to prevent the binding of VEGF-$A_{165}$ to heparin raised the possibility that the inhibitory activity of this compound might be dependent upon its interaction with VEGF-HBD.

To address this hypothesis, HUVECs were challenged in parallel with VEGF-$A_{165}$ or VEGF-$A_{121}$ isoforms in the absence or in the presence of increasing concentrations of BOC2. As shown in Fig. 3a-f, BOC2 confirmed its capacity to prevent VEGFR2 phosphorylation, HUVEC proliferation and sprouting triggered by VEGF-$A_{165}$ whereas it did not exert any inhibitory activity when HUVECs were stimulated by VEGF-$A_{121}$. Accordingly, BOC2 did not affect the binding of VEGF-$A_{121}$, as well as of the non-heparin binding VEGF family member VEGF-E [37], to sVEGFR2 immobilized

to a BIAcore sensor chip when tested under the same experimental conditions effective for VEGF-$A_{165}$/VEGFR2 interaction (Fig. 3g). Taken together, these data support the hypothesis that BOC2 may exert its anti-VEGF-$A_{165}$ action by targeting the polycationic surface on VEGF-HBD.

On this basis, a molecular modeling approach was used to investigate putative BOC2/VEGF-HBD interactions. Induced-fit docking (IFD) simulations [31] using the X-ray coordinates of VEGF-HBD [34] showed, among possible solutions, two binding poses in which BOC2 interacted with the polycationic surface of VEGF-HBD (Supplementary Fig. S2). These poses differed mainly for the accommodation of the C-terminal Phe residue whose free carboxylate targets Arg35 and Arg39 in pose I and Arg49 in pose II.

As these two binding models possess similar IFD scores (*i.e.*, pose I: 119.9 kcal $mol^{-1}$; pose II: 119.7 kcal $mol^{-1}$), we examined their structural stability using molecular dynamics (MD) simulations. MD simulations showed that the accommodation of BOC2 in binding pose I is unstable, as this peptide leaved VEGF-HBD and reached an unbound state after 60 ns only of simulations (Supplementary Fig. S3). At variance, BOC2 remained anchored to VEGF-HBD for at least 300 ns in binding pose II (Supplementary Fig. S3), acquiring a stable arrangement (Supplementary Fig. S4). In this simulation, BOC2 assumed an extended conformation, which allowed it to cover large part of the basic surface of VEGF-HBD. This pose is stabilized by a series of specific interactions (Fig. 4 and Supplementary Fig. S5) that included: *i*. electrostatic interactions formed by the free-carboxylate group of the C-terminal Phe residue of BOC2 and the side chains of Arg49 and Arg14; *ii*. a persistent H-bond formed by BOC2 backbone with Asp51 *plus* other transient H-bonds (*e.g.* between backbone groups of BOC2 and VEGF-HBD); *iii.* cation-$\pi$ interactions undertaken by the N-terminal Phe residue of BOC2 with Arg39 of VEGF-HBD.

Thus, molecular modeling of BOC2/VEGF-HBD interactions suggests that the lipophilic small molecule BOC2 may accommodate in VEGF-HBD close to basic regions recognized by sulfated GAGs, thus preventing VEGF-$A_{165}$/heparin interaction and biological activity. Notably, this capacity does not appear to be limited to VEGF-$A_{165}$. Indeed, BOC2 is able to prevent the interaction of a variety of heparin-binding angiogenic growth factors with heparin immobilized to a BIAcore sensorchip, including the prototypic heparin-binding angiogenic growth factor FGF2 (Supplementary Fig S6A). In keeping with a competitive mechanism of action, an inverse correlation appears to exist between the capacity of BOC2 to hamper the interaction of the various proteins with immobilized heparin (expressed as $ID_{50}$ value) and their affinity for the immobilized GAG (expressed as $K_d$ value) (Supplementary Fig. S6B), BOC2 being usually more effective on

those proteins showing a weaker interaction with the heparin chip. In conclusion, BOC2 acts as a multi-target binder for a variety of heparin-binding angiogenic factors.

**BOC2 inhibits the angiogenic activity of FGF2**

The above observations prompted us to assess whether BOC2 is able to inhibit also the angiogenic potential of the heparin-binding angiogenic growth factor FGF2 [10]. As observed for VEGF-$A_{165}$, BOC2 inhibits FGFR1 phosphorylation and activation of the downstream secondary signaling mediators $EKR_{1/2}$ and AKT in FGFR1-overexpressing bovine endothelial GM7373-flg cells [23] (Fig. 5a-d).

Accordingly, BOC2 inhibits the binding of FGF2 to sFGFR1 immobilized to a BIAcore sensor chip (Fig. 5e) and FGF2-mediated HUVEC proliferation and sprouting of fibrin-embedded HUVEC spheroids (Fig. 5f,g).

On this basis, we assessed the capacity of BOC2 to inhibit the angiogenic activity exerted by highly metastatic human melanoma A2058 cells and of human prostate cancer DU145 cells. These tumor cell lines were chosen for their capacity to express high levels of both VEGF-A and FGF2 (Fig. 6a). As shown in Fig. 6b,c, the conditioned medium from both cell lines induced HUVEC proliferation and sprouting that were abrogated by BOC2. Accordingly, BOC2 was able to suppress in both assays the biological activity exerted by the co-administration of optimal concentrations of VEGF-$A_{165}$ *plus* FGF2. In keeping with these observations, BOC2 inhibits neovessel formation induced *in vivo* by A2058 and DU145 tumor cells grafted on the top of the chick embryo CAM (Fig. 6d,e).

## Discussion

BOC2 pentapeptide is a well-known FPR1/FPR2 antagonist [15] that has been widely used as a tool to assess the role of FPRs in physiological and pathological conditions [15,17]. Here, we demonstrate that BOC2 may act also as a multi-heparin binding growth factor inhibitor due to its capacity to hamper the interaction of various heparin-binding angiogenic modulators with heparin/HSPGs. Accordingly, BOC2 inhibits the activity of the prototypic heparin-binding angiogenic factors VEGF-$A_{165}$ and FGF2. Due to this ability, BOC2 inhibits the angiogenic activity of VEGF-A/FGF2-expressing human tumor cells *in vitro* and *in vivo*.

The inhibitory effect of BOC2 appears to be specific: i) BOC2 does not affect the activity of the non-heparin binding VEGF-$A_{121}$ isoform; ii) the related FPR inhibitor BOC1 and the control BOC-F-OH molecule are ineffective.

The capacity of BOC2 to hamper the interaction of VEGF-$A_{165}$ with immobilized heparin and to affect the activity of VEGF-$A_{165}$ but not of the VEGF-$A_{121}$ isoform raised the hypothesis that BOC2 may bind the heparin-binding domain VEGF-HBD of the VEGF-$A_{165}$ molecule. Compounds different from sulfated GAGs had already been shown to bind VEGF-$A_{165}$ and competing with heparin for its binding site, thus inhibiting VEGFR2 activation. For instance, carboxymethyl benzylamide dextran was shown to reduce $^{125}$I-VEGF-$A_{165}$ binding to coated heparin-albumin and to prevent $VEGF_{165}$-induced VEGF2 autophosphorylation [38].

Docking simulations and molecular dynamics confirmed that BOC2 might interact with VEGF-HBD, taking stable attractive interactions. In particular, one structurally and energetically stable binding pose has been identified that may account for the ability of BOC2 to interact with critical basic residues at the polycationic surface of VEGF-HBD involved in the recognition of sulfated GAGs (*i.e.* Arg14, Arg35, Arg39, Arg49). MD simulations have shown that BOC2 remains tightly bound to the VEGF-HBD surface for at least 300 ns in this pose. Visual inspection of representative snapshots taken from the MD simulations indicates that nearly all the BOC2 residues are important for VEGF-HBD binding. Indeed, in addition to the favorable polar interactions formed by the free-carboxylate group of the C-terminal Phe residue with the side chains of Arg49 and Arg14 (Supplementary Fig. S5), the overall structure of BOC2 backbone forms a series of stable and transient H-bonds with the VEGF-HBD surface, including those formed with Asp51 side chain and Arg49 backbone (Fig. 4 and Supplementary Fig. S5). Moreover, the N-terminal Phe of BOC2 undertakes cation-π interactions with Arg39 of the VEGF-HBD, while its N-tert-butyloxycarbonyl group forms Van der Waals interactions in a channel delimited by hydrophobic residues (*e.g.* Leu17). Given the weak nature of each interaction between BOC2 and VEGF-HBD, it is conceivable that the binding affinity may result from the cooperation among all these interactions. This may explain the lack of anti-$VEGF_{165}$ activity of compounds lacking some interaction points, such as BOC1 and BOC-F-OH.

It is worth mentioning that the accommodation of aromatic small molecules close to basic regions involved in the recognition of carbohydrate sulfates has already been observed in some crystal structures. This is the case of a tetrahydroisoquinoline compound able to bind the hyaluron binding domain of the CD44 receptor [39] or of the 2-([1,1'-biphenyl]-2-ylmethyl)malonic acid molecule able to bind the chondroitin sulfate-binding region of cathepsin K [40]. Thus, despite its lipophilic nature, BOC2 appears to be capable of undertaking several contacts with the surface of the VEGF-HBD domain. The observation that BOC2 inhibits the binding to immobilized heparin of various

heparin-binding growth factors structurally unrelated to VEGF-$A_{165}$, being usually more effective toward those factors showing a weaker interaction with the GAG, further supports this hypothesis.

HSPGs are known to mediate the binding of VEGF-$A_{165}$ to its signaling receptor VEGFR2, leading to the formation of bioactive HSPG/VEGF-$A_{165}$/VEGFR2 ternary complexes [8]. SPR experiments show that BOC2 hampers the formation of this complex by preventing VEGF-$A_{165}$ binding to both HSPGs and VEGFR2. It is conceivable that the association of BOC2 with the VEGF-HBD region may cause a conformational rearrangement of VEGF-$A_{165}$, resulting in the loss of its ability to interact properly with VEGFR2. Likewise, BOC2 inhibits the binding of FGF2 to immobilized heparin and FGFR1. A similar mechanism of action has been described for thrombospondin-derived small molecule FGF2 antagonists that engage the heparin-binding site of FGF2, inducing long-range dynamics perturbations along the FGF2/FGFR1 interface [41,42]. Further studies are required to elucidate this hypothesis.

The capacity of BOC2 to act as a multi-heparin-binding growth factor antagonist advocates caution about the interpretation of FPR-focusing experimental data obtained with this compound. For instance, previous observations from our laboratory had shown that BOC2 inhibits the angiogenic activity of the vitreous humor obtained from PDR patients, suggesting a possible involvement of FPRs in this disease [18]. However, our novel findings cast some doubts on this hypothesis, the effect of BOC2 on the angiogenic activity of PDR vitreous being possibly due to its FPR-independent effects. Indeed, pan-heparin-binding growth factor antagonists inhibit the angiogenic responses induced by PDR vitreous in pre-clinical settings [12] and anti-VEGF agents are widely used in PDR therapy [22].

BOC2 hampers the angiogenic activity exerted by highly metastatic human melanoma A2058 cells and human prostate cancer DU145 cells that co-express VEGF-A and FGF2. Thus, due to its multi-heparin-binding growth factor capacity, BOC2 may represent the basis for the design of novel multi-target inhibitors for the therapy of angiogenesis-dependent diseases, including cancer.

**References**

1. Carmeliet P (2003) Angiogenesis in health and disease. Nat Med 9:653-660.

2. Witmer AN, Vrensen GF, Van Noorden CJ, Schlingemann RO (2003) Vascular endothelial growth factors and angiogenesis in eye disease. Prog Retin Eye Res 22:1-29.

3. Elshabrawy HA, Chen Z, Volin MV, Ravella S, Virupannavar S, Shahrara S (2015) The pathogenic role of angiogenesis in rheumatoid arthritis. Angiogenesis 18:433-448.

4. Seabrook TJ, Littlewood-Evans A, Brinkmann V, Pollinger B, Schnell C, Hiestand PC (2010) Angiogenesis is present in experimental autoimmune encephalomyelitis and pro-angiogenic factors are increased in multiple sclerosis lesions. J Neuroinflammation 7:95.

5. Weis SM, Cheresh DA (2011) Tumor angiogenesis: molecular pathways and therapeutic targets. Nat Med 17:1359-1370.

6. Bergers G, Benjamin LE (2003) Tumorigenesis and the angiogenic switch. Nat Rev Cancer 3:401-410.

7. Jayson GC, Kerbel R, Ellis LM, Harris AL (2016) Antiangiogenic therapy in oncology: current status and future directions. Lancet 388:518-529.

8. Chiodelli P, Bugatti A, Urbinati C, Rusnati M (2015) Heparin/Heparan sulfate proteoglycans glycomic interactome in angiogenesis: biological implications and therapeutical use. Molecules 20:6342-6388.

9. Koch S, Claesson-Welsh L (2012) Signal transduction by vascular endothelial growth factor receptors. Cold Spring Harb Perspect Med 2:a006502.

10. Presta M, Dell'Era P, Mitola S, Moroni E, Ronca R, Rusnati M (2005) Fibroblast growth factor/fibroblast growth factor receptor system in angiogenesis. Cytokine Growth Factor Rev 16:159-178.

11. Leali D, Belleri M, Urbinati C, Coltrini D, Oreste P, Zoppetti G et al. (2001) Fibroblast growth factor-2 antagonist activity and angiostatic capacity of sulfated Escherichia coli K5 polysaccharide derivatives. J Biol Chem 276:37900-37908.

12. Rezzola S, Dal Monte M, Belleri M, Bugatti A, Chiodelli P, Corsini M et al. (2015) Therapeutic Potential of Anti-Angiogenic Multitarget N,O-Sulfated E. Coli K5 Polysaccharide in Diabetic Retinopathy. Diabetes 64:2581-2592.

13. Koch S, Tugues S, Li X, Gualandi L, Claesson-Welsh L (2011) Signal transduction by vascular endothelial growth factor receptors. Biochem J 437:169-183.

14. Teran M, Nugent MA (2015) Synergistic Binding of Vascular Endothelial Growth Factor-A and Its Receptors to Heparin Selectively Modulates Complex Affinity. J Biol Chem 290:16451-16462.

15. Toniolo C, Bonora GM, Showell H, Freer RJ, Becker EL (1984) Structural requirements for formyl homooligopeptide chemoattractants. Biochemistry 23:698-704.
16. Prevete N, Liotti F, Marone G, Melillo RM, de Paulis A (2015) Formyl peptide receptors at the interface of inflammation, angiogenesis and tumor growth. Pharmacol Res 102:184-191.
17. Lee HY, Lee M, Bae YS (2017) Formyl Peptide Receptors in Cellular Differentiation and Inflammatory Diseases. J Cell Biochem 118:1300-1307.
18. Rezzola S, Corsini M, Chiodelli P, Cancarini A, Nawaz IM, Coltrini D et al. (2017) Inflammation and N-formyl peptide receptors mediate the angiogenic activity of human vitreous humour in proliferative diabetic retinopathy. Diabetologia 60:719-728.
19. Simo R, Carrasco E, Garcia-Ramirez M, Hernandez C (2006) Angiogenic and antiangiogenic factors in proliferative diabetic retinopathy. Curr Diabetes Rev 2:71-98.
20. Wang S, Park JK, Duh EJ (2012) Novel targets against retinal angiogenesis in diabetic retinopathy. Curr Diab Rep 12:355-363.
21. Dai Y, Wu Z, Wang F, Zhang Z, Yu M (2014) Identification of chemokines and growth factors in proliferative diabetic retinopathy vitreous. Biomed Res Int 2014:486386.
22. Bandello F, Lattanzio R, Zucchiatti I, Del Turco C (2013) Pathophysiology and treatment of diabetic retinopathy. Acta Diabetol 50:1-20.
23. Tanghetti E, Ria R, Dell'Era P, Urbinati C, Rusnati M, Ennas MG, Presta M (2002) Biological activity of substrate-bound basic fibroblast growth factor (FGF2): recruitment of FGF receptor-1 in endothelial cell adhesion contacts. Oncogene 21:3889-3897.
24. Kimmel CB, Ballard WW, Kimmel SR, Ullmann B, Schilling TF (1995) Stages of embryonic development of the zebrafish. Dev Dyn 203:253-310.
25. Nicoli S, De Sena G, Presta M (2009) Fibroblast growth factor 2-induced angiogenesis in zebrafish: the zebrafish yolk membrane (ZFYM) angiogenesis assay. J Cell Mol Med 13:2061-2068.
26. Nicoli S, Presta M (2007) The zebrafish/tumor xenograft angiogenesis assay. Nat Protoc 2:2918-2923.
27. Nicoli S, Ribatti D, Cotelli F, Presta M (2007) Mammalian tumor xenografts induce neovascularization in zebrafish embryos. Cancer Res 67:2927-2931.
28. Mitola S, Moroni E, Ravelli C, Andres G, Belleri M, Presta M (2008) Angiopoietin-1 mediates the pro-angiogenic activity of the bone morphogenic protein antagonist Drm. Blood 112:1154-1157.
29. Harder E, Damm W, Maple J, Wu C, Reboul M, Xiang JY et al. (2016) OPLS3: A Force Field Providing Broad Coverage of Drug-like Small Molecules and Proteins. J Chem Theory Comput 12:281-296.

30. Parker MW, Xu P, Li X, Vander Kooi CW (2012) Structural basis for selective vascular endothelial growth factor-A (VEGF-A) binding to neuropilin-1. J Biol Chem 287:11082-11089.
31. Sherman W, Day T, Jacobson MP, Friesner RA, Farid R (2006) Novel procedure for modeling ligand/receptor induced fit effects. J Med Chem 49:534-553.
32. Krilleke D, DeErkenez A, Schubert W, Giri I, Robinson GS, Ng YS, Shima DT (2007) Molecular mapping and functional characterization of the VEGF164 heparin-binding domain. J Biol Chem 282:28045-28056.
33. Loncharich RJ, Brooks BR, Pastor RW (1992) Langevin dynamics of peptides: the frictional dependence of isomerization rates of N-acetylalanyl-N'-methylamide. Biopolymers 32:523-535.
34. Darden T, York D, Pedersen L (1993) Particle Mesh Ewald - an N.Log(N) Method for Ewald Sums in Large Systems. Journal of Chemical Physics 98:10089-10092.
35. Mitola S, Ravelli C, Moroni E, Salvi V, Leali D, Ballmer-Hofer K et al. (2010) Gremlin is a novel agonist of the major proangiogenic receptor VEGFR2. Blood 116:3677-3680.
36. Pisano C, Aulicino C, Vesci L, Casu B, Naggi A, Torri G et al. (2005) Undersulfated, low-molecular-weight glycol-split heparin as an antiangiogenic VEGF antagonist. Glycobiology 15:1C-6C.
37. Ogawa S, Oku A, Sawano A, Yamaguchi S, Yazaki Y, Shibuya M (1998) A novel type of vascular endothelial growth factor, VEGF-E (NZ-7 VEGF), preferentially utilizes KDR/Flk-1 receptor and carries a potent mitotic activity without heparin-binding domain. J Biol Chem 273:31273-31282.
38. Hamma-Kourbali Y, Vassy R, Starzec A, Le Meuth-Metzinger V, Oudar O, Bagheri-Yarmand R et al. (2001) Vascular endothelial growth factor 165 (VEGF(165)) activities are inhibited by carboxymethyl benzylamide dextran that competes for heparin binding to VEGF(165) and VEGF(165).KDR Complexes. J Biol Chem 276:39748-39754.
39. Liu LK, Finzel BC (2014) Fragment-based identification of an inducible binding site on cell surface receptor CD44 for the design of protein-carbohydrate interaction inhibitors. J Med Chem 57:2714-2725.
40. Novinec M, Rebernik M, Lenarcic B (2016) An allosteric site enables fine-tuning of cathepsin K by diverse effectors. FEBS Lett 590:4507-4518.
41. Colombo G, Margosio B, Ragona L, Neves M, Bonifacio S, Annis DS et al. (2010) Non-peptidic thrombospondin-1 mimics as fibroblast growth factor-2 inhibitors: an integrated strategy for the development of new antiangiogenic compounds. J Biol Chem 285:8733-8742.

42. Pinessi D, Foglieni C, Bugatti A, Moroni E, Resovi A, Ribatti D et al. (2016) PO-15 - Antiangiogenic small molecule ligands of FGF2 derived from the endogenous inhibitor thrombospondin-1. Thrombosis Research 140 Suppl 1:S182.

## Figure legends

**Fig. 1** BOC2 inhibits the angiogenic activity of VEGF-$A_{165}$. **a** HUVECs were treated for 10 min with vehicle (untreated) or with 30 ng/mL VEGF-$A_{165}$ and increasing concentrations of BOC2. Then, cell extracts were probed with anti-pVEGFR2, anti-p$ERK_{1/2}$ and anti-pAKT antibodies. **b-d** Densitometric analysis of pVEGFR2 (**b**), p$ERK_{1/2}$ (**c**) and pAKT (**d**) immunoreactive bands normalized to the expression levels of FAK, total $ERK_2$ or α-tubulin, as indicated. Data are the mean ± SEM of 2 independent experiments. **e** HUVECs were treated with VEGF-$A_{165}$ in the presence of increasing concentrations of BOC1 (upper panel) or BOC-H-OH (lower panel) and cell extracts were probed with anti-pVEGFR2 antibody. **f** Densitometric analysis of pVEGFR2 activation in HUVECs treated with VEGF-$A_{165}$ and increasing concentration of BOC2 (white circles), BOC1 (black circles), or BOC-H-OH (black squares). Data are the mean ± SEM of 4 independent experiments. **g** HUVEC proliferation assay. HUVECs were stimulated with VEGF-$A_{165}$ and increasing concentration of BOC2 (white circles), BOC1 (black circles) and BOC-H-OH (black squares). After 48 h, cells were counted and data (mean ± SEM of 3 independent experiments) represented as percentage of VEGF-$A_{165}$ activity. **h, i** HUVEC sprouting assay. **h** HUVEC spheroids embedded in fibrin gel were incubated with 30 ng/mL VEGF-$A_{165}$ in the presence of increasing concentrations of BOC2, BOC1, or BOC-F-OH. After 24 h, the number of radially growing sprouts were counted and data (mean ± SEM of 3 independent experiments) represented as percentage of VEGF-$A_{165}$ activity. **i** Representative images of VEGF-$A_{165}$-treated spheroids in the absence (upper panel) or in the presence (lower panel) of 60 µM BOC2. **j, k** ZFYM angiogenesis assay. **j** Two nL of PBS (vehicle) or VEGF-$A_{165}$ (40 ng/embryo) were injected into the perivitelline space of zebrafish embryos at 48 hpf. After 2 h, 4 nL of increasing concentrations of BOC2 were injected in the blood stream of embryos. After 24 h of incubation, the length of subintestinal vessels (ISVs) was measured. **k** Representative images of the formation of ISVs in VEGF-$A_{165}$-injected zebrafish embryos in the absence (upper panel) or in the presence (lower panel) of 10 pmoles/embryo of BOC2. Data are the mean ± SEM of 2 independent experiments. *P < 0.05, **P < 0.01 and ***P < 0.001 vs. VEGF-$A_{165}$ (ANOVA).

**Fig. 2** BOC2 inhibits the formation of HSPG/VEGF-$A_{165}$/VEGFR2 ternary complexes. **a** Cell-cell adhesion assay. HSPG-deficient ECD-VEGFR2-YFP A745 CHO cells were added to HSPG-bearing CHO-K1 monolayers in the presence of VEGF-$A_{165}$ (75 ng/mL) and increasing concentrations of BOC2. Data are the mean ± SEM of 6 microscopic fields. **b, c** SPR analysis. VEGF-$A_{165}$ (100 nM) was co-injected with increasing concentrations of BOC2 (white circles) or BOC1 (black circles) on BIAcore sensorchips coated with immobilized sVEGFR2 (**b**) or heparin

(**c**). The response (in RU) was recorded at the end of each injection and plotted as a function of peptide concentration. Data are the mean ± SEM of 2 independent experiments. *P < 0.05, **P < 0.01 and ***P < 0.001 vs. VEGF- $A_{165}$ (ANOVA).

**Fig. 3** BOC2 does not affect the activity of $VEGFA_{121}$. **a, c** HUVECs were treated for 10 min with 30 ng/mL VEGF-$A_{165}$ (**a**) or VEGF-$A_{121}$ (**c**) in the absence or presence of 120 μM BOC2. Then, cell extracts were probed with an anti-pVEGFR2 antibody. **b, d** Corresponding densitometric analysis of pVEGFR2 immunoreactive bands normalized to the expression levels of FAK. Data are the mean ± SEM of 3 independent experiments. **e** HUVEC proliferation assay. HUVECs were stimulated for 24 h with 30 ng/mL of $VEGFA_{121}$ (black circles) or VEGF-$A_{165}$ (white circles) and increasing concentrations of BOC2. After 48 h, cells were counted and data (mean ± SEM of 3 independent experiments) were represented as percentage of VEGF activity. **f** HUVEC sprouting assay. HUVEC spheroids embedded in fibrin gel were incubated with 30 ng/mL of $VEGFA_{121}$ (black circles) or VEGF-$A_{165}$ (white circles) in the presence of increasing concentrations of BOC2. HUVECs sprouts were counted and data (mean ± SEM of 3 independent experiments) are represented as percentage of VEGF activity. **g** SPR analysis. $VEGFA_{121}$ (black circles), VEGF-$A_{165}$ (white circles) or VEGF-E (black square) (all at 150 nM) were co-injected with increasing concentrations of BOC2 on a BIAcore sensorchip coated with immobilized sVEGFR2. The response (in RU) was recorded at the end of each injection and plotted as a function of BOC2 concentration. *P < 0.05, **P < 0.01 and ***P < 0.001 vs. VEGF (ANOVA).

**Fig. 4** Molecular modeling of BOC2/VEGF-HBD interaction. VEGF-HBD (grey carbon atoms) in complex with BOC2 (green carbon atoms) in a snapshot at the end of a 300-ns long MD simulation. The molecular surface of VEGF-HBD is depicted with positively charged regions colored in blue, negatively regions in red and neutrals region in white. Arginine residues involved in the recognition of heparan sulfate and Asp51, interacting with BOC2, are labelled.

**Fig. 5** BOC2 inhibits the activity of FGF2. **a** Endothelial GM7373-flg cells were treated for 20 min with vehicle (untreated) or with 30 ng/mL FGF2 and increasing concentrations of BOC2. Then, cell extracts were probed with anti-pFGFR1, anti-$pERK_{1/2}$ and anti-pAKT antibodies. **b-d** Densitometric analysis of pFGFR1 (**b**), $pERK_{1/2}$ (**c**) and pAKT (**d**) immunoreactive bands normalized to the expression levels of α-tubulin. Data are the mean ± SEM of 2 independent experiments. **e** SPR analysis. FGF2 (100 nM) was co-injected with increasing concentrations of BOC2 on a BIAcore sensorchip coated with immobilized sFGFR1. The response (in RU) was recorded at the end of injection and plotted as a function of BOC2 concentration. Data are the mean ± SEM of 2 independent experiments. **f** Cell proliferation assay. GM7373-flg cells were stimulated

with 30 ng/mL of FGF2 and increasing concentrations of BOC2. After 48 h, cells were counted and data (mean ± SEM of 3 independent experiments) are represented as percentage of FGF2 activity. **g** HUVEC sprouting assay. HUVEC spheroids embedded in fibrin gel were incubated with 30 ng/mL of FGF2 in the presence of increasing concentrations of BOC2. The formation of radially growing sprouts was counted after 24 h and data (mean ± SEM of 3 independent experiments) are represented as the percentage of VEGF activity. **P < 0.01 and ***P < 0.001 vs. FGF2 (ANOVA).

**Fig. 6** BOC2 inhibits the angiogenic activity of human cancer cells. **a** Semi-quantitative RT-PCR analysis of *VEGF* and *FGF2* gene expression in human melanoma A2058 and prostate cancer DU145 cell lines. The expression levels of *GAPDH* were used as internal control. **b** HUVEC proliferation assay. HUVECs were incubated with the conditioned medium (CM) from A2058 or DU145 cells (both at 1:4 dilution, v/v) or with fresh medium added with 30 ng/mL VEGF-$A_{165}$ *plus* 30 ng/mL FGF2 in the absence or in the presence of 60 μM BOC2. Cells were counted after 48 h. **c** HUVEC sprouting assay. HUVEC spheroids embedded in fibrin gel were treated as in **b** and the formation of radially growing sprouts was counted after 24 h. Data, normalized to the activity of media without BOC2, are the mean ± SEM of 2 independent experiments. **d, e** Chick embryo CAM assay. Number of neovessels/implant (n = 14) infiltrating the CAM mesenchyme (**d**) induced by A2058 or DU145 cancer cells in the absence or in the presence BOC2. **e** Representative images of CAMs grafted with A2058 cells in the absence (upper panel) or in the presence (lower panel) of 60 μM BOC2. Data are the mean ± SEM of 2 experiments. **P < 0.01 and ***P < 0.001 vs. untreated (ANOVA).

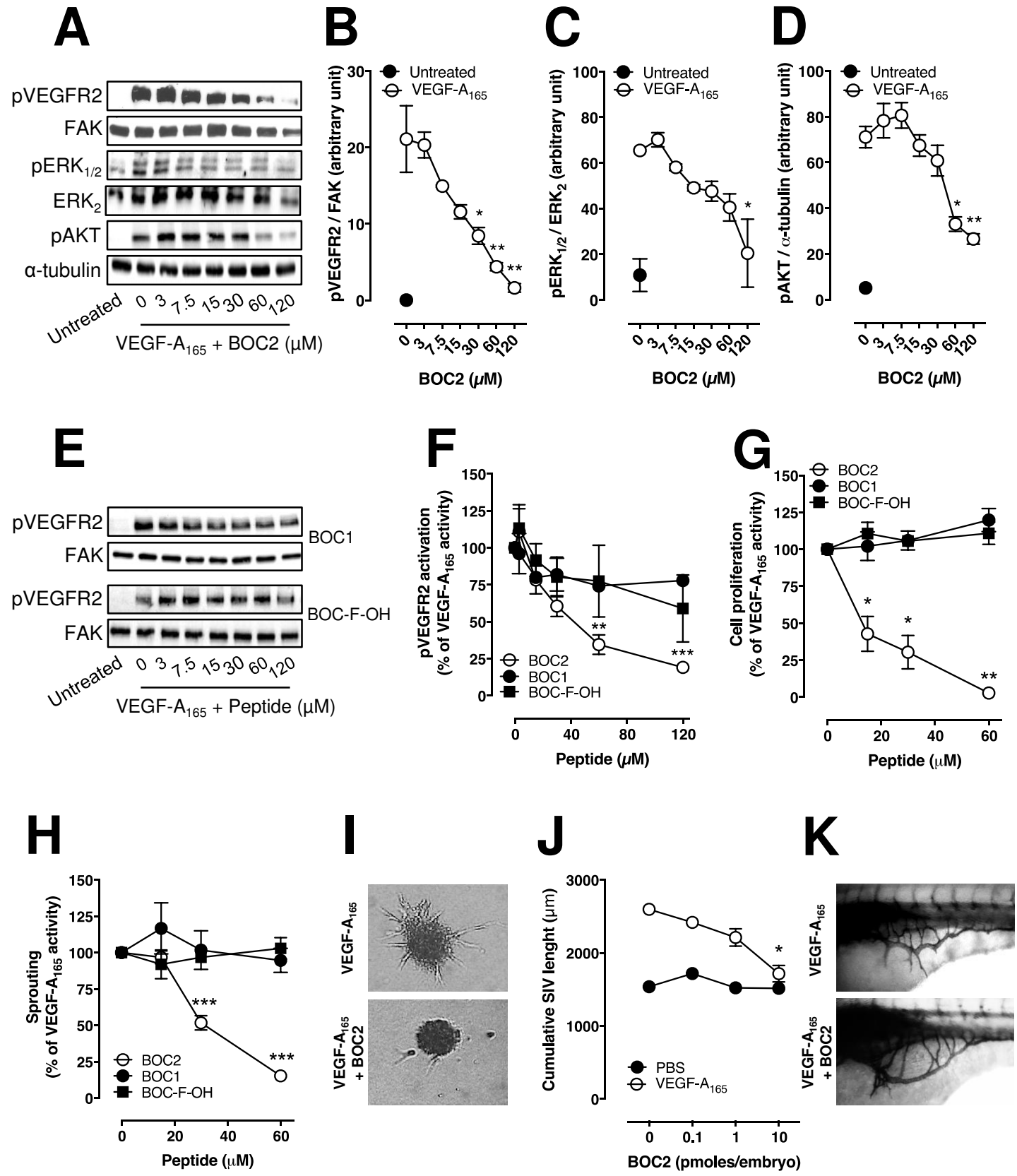
A
pVEGFR2
FAK
pERK1/2
ERK2
pAKT
α-tubulin
Untreated
0 3 7.5 15 30 60 120
VEGF-A165 + BOC2 (μM)
B
pVEGFR2 / FAK (arbitrary unit)
Untreated
VEGF-A165
BOC2 (μM)
C
pERK1/2 / ERK2 (arbitrary unit)
Untreated
VEGF-A165
BOC2 (μM)
D
pAKT / α-tubulin (arbitrary unit)
Untreated
VEGF-A165
BOC2 (μM)
E
pVEGFR2
FAK
BOC1
pVEGFR2
FAK
BOC-F-OH
Untreated
0 3 7.5 15 30 60 120
VEGF-A165 + Peptide (μM)
F
pVEGFR2 activation
(% of VEGF-A165 activity)
BOC2
BOC1
BOC-F-OH
Peptide (μM)
G
Cell proliferation
(% of VEGF-A165 activity)
BOC2
BOC1
BOC-F-OH
Peptide (μM)
H
Sprouting
(% of VEGF-A165 activity)
BOC2
BOC1
BOC-F-OH
Peptide (μM)
I
VEGF-A165
VEGF-A165 + BOC2
J
Cumulative SIV lenght (μm)
PBS
VEGF-A165
BOC2 (pmoles/embryo)
K
VEGF-A165
VEGF-A165 + BOC2

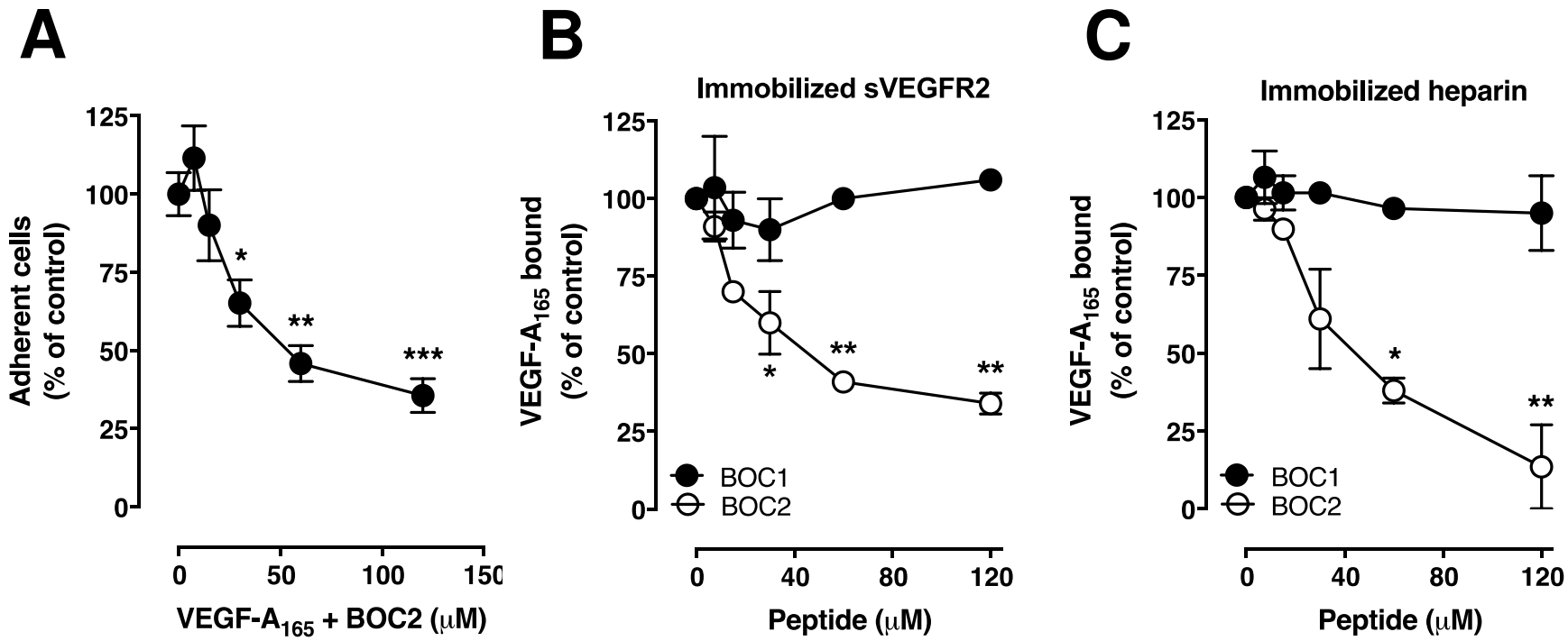
A
Adherent cells
(% of control)
125
100
75
50
25
0
*
**
***
0
50
100
150
VEGF-A165 + BOC2 (μM)
B
Immobilized sVEGFR2
VEGF-A165 bound
(% of control)
125
100
75
50
25
0
*
**
**
BOC1
BOC2
0
40
80
120
Peptide (μM)
C
Immobilized heparin
VEGF-A165 bound
(% of control)
125
100
75
50
25
0
*
**
BOC1
BOC2
0
40
80
120
Peptide (μM)

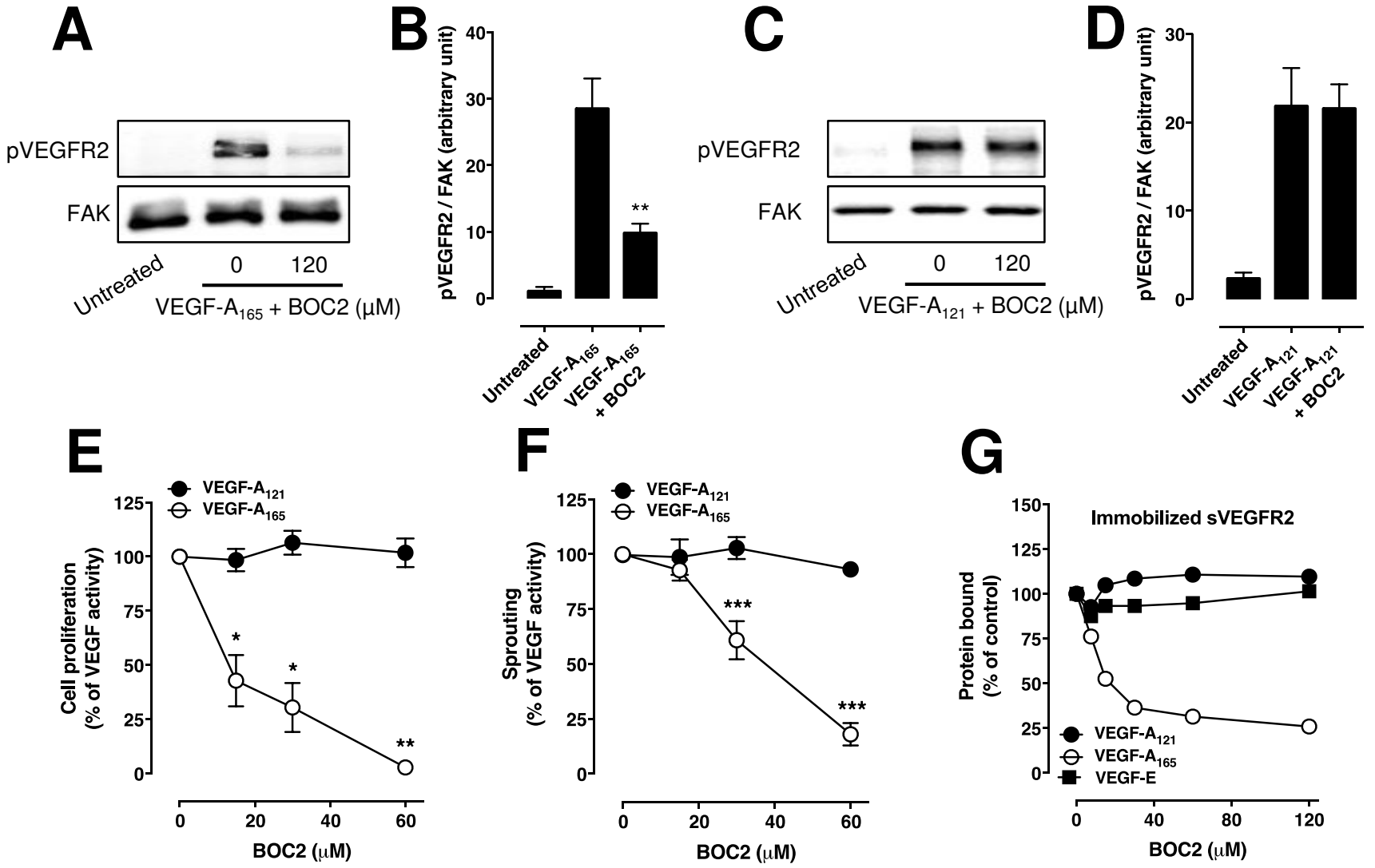
A
pVEGFR2
FAK
Untreated
0
120
VEGF-A165 + BOC2 (μM)
B
pVEGFR2 / FAK (arbitrary unit)
40
30
20
10
0
**
Untreated
VEGF-A165
VEGF-A165 + BOC2
C
pVEGFR2
FAK
Untreated
0
120
VEGF-A121 + BOC2 (μM)
D
pVEGFR2 / FAK (arbitrary unit)
30
20
10
0
Untreated
VEGF-A121
VEGF-A121 + BOC2
E
VEGF-A121
VEGF-A165
Cell proliferation (% of VEGF activity)
125
100
75
50
25
0
*
*
**
0
20
40
60
BOC2 (μM)
F
VEGF-A121
VEGF-A165
Sprouting (% of VEGF activity)
125
100
75
50
25
0
***
***
0
20
40
60
BOC2 (μM)
G
Immobilized sVEGFR2
Protein bound (% of control)
150
125
100
75
50
25
0
VEGF-A121
VEGF-A165
VEGF-E
0
40
80
120
BOC2 (μM)

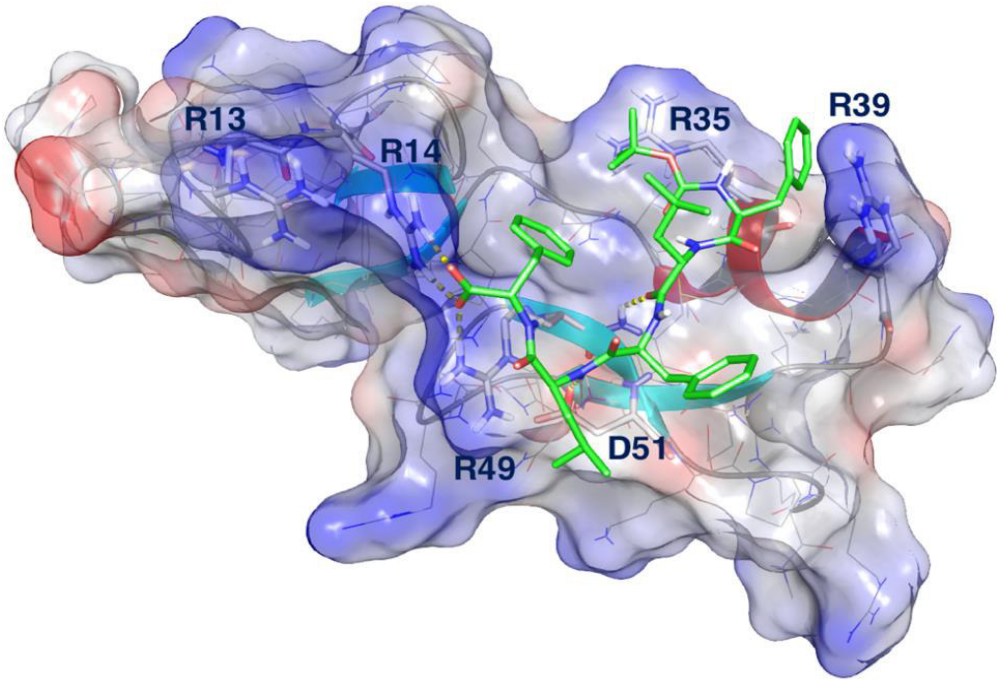
R13
R14
R35
R39
R49
D51

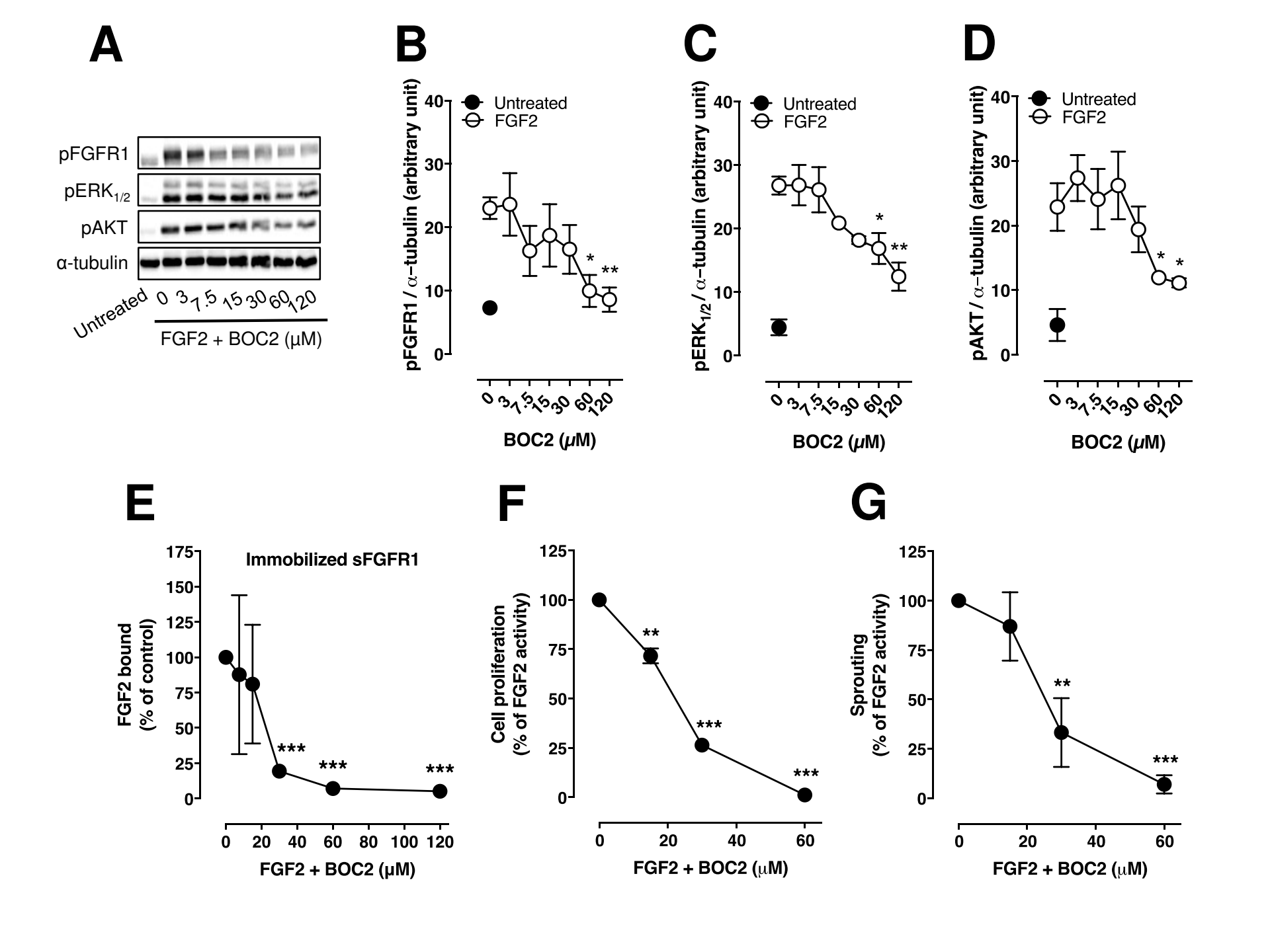
A
pFGFR1
pERK1/2
pAKT
α-tubulin
Untreated
0 3 7.5 15 30 60 120
FGF2 + BOC2 (μM)
B
pFGFR1 / α–tubulin (arbitrary unit)
Untreated
FGF2
BOC2 (μM)
C
pERK1/2 / α–tubulin (arbitrary unit)
Untreated
FGF2
BOC2 (μM)
D
pAKT / α–tubulin (arbitrary unit)
Untreated
FGF2
BOC2 (μM)
E
Immobilized sFGFR1
FGF2 bound (% of control)
FGF2 + BOC2 (μM)
F
Cell proliferation (% of FGF2 activity)
FGF2 + BOC2 (μM)
G
Sprouting (% of FGF2 activity)
FGF2 + BOC2 (μM)

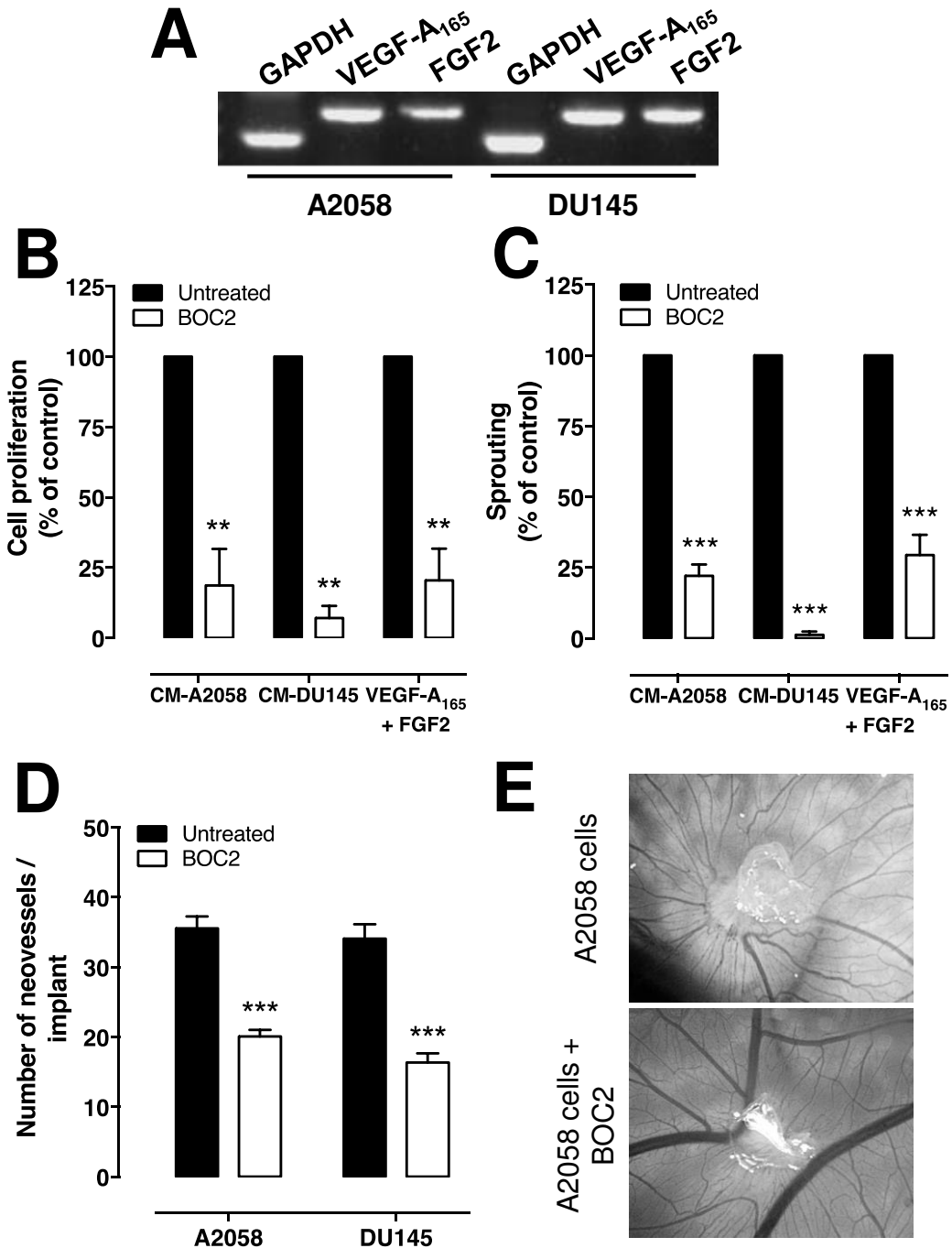
A
GAPDH
VEGF-A165
FGF2
GAPDH
VEGF-A165
FGF2
A2058
DU145
B
Untreated
BOC2
Cell proliferation (% of control)
125
100
75
50
25
0
**
**
**
CM-A2058
CM-DU145
VEGF-A165 + FGF2
C
Untreated
BOC2
Sprouting (% of control)
125
100
75
50
25
0
***
***
***
CM-A2058
CM-DU145
VEGF-A165 + FGF2
D
Untreated
BOC2
Number of neovessels / implant
50
40
30
20
10
0
***
***
A2058
DU145
E
A2058 cells
A2058 cells + BOC2

# *N*-tert-butyloxycarbonyl-Phe-Leu-Phe-Leu-Phe (BOC2) inhibits the angiogenic activity of heparin-binding growth factors.

**Cellular and Molecular Life Sciences**

Imtiaz M. Nawaz[1], Paola Chiodelli[1], Sara Rezzola[1], Giuseppe Paganini[1], Michela Corsini[1], Alessio Lodola[2], Alessio Di Ianni [2], Marco Mor[2] and Marco Presta[1]

[1] Department of Molecular and Translational Medicine, University of Brescia, Italy

[2] Department of Food and Drug, University of Parma, Italy.

Correspondence to: Marco Presta (marco.presta@unibs.it)

## Supplementary Figures

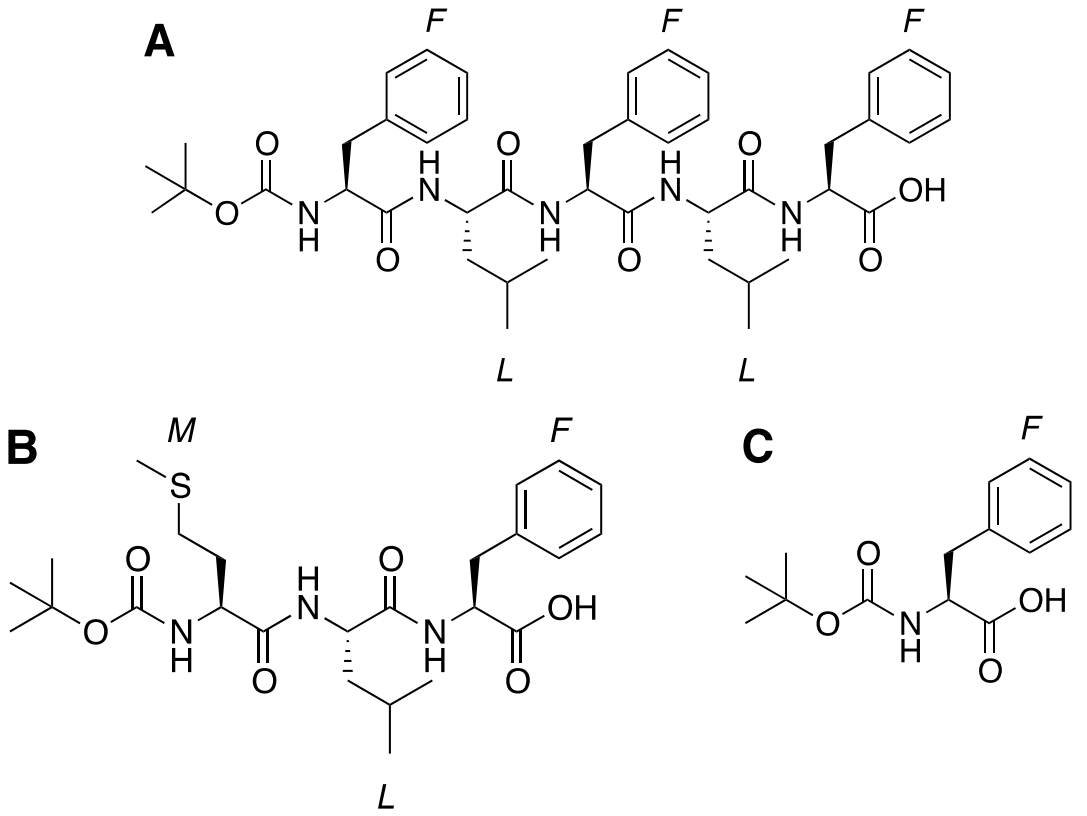


**Figure S1.** Chemical structures of BOC2 (**A**), BOC1 (**B**) and BOC-F-OH (**C**). Structures were drawn using ChemDraw ultra 12.0 V software, CambridgeSoft.

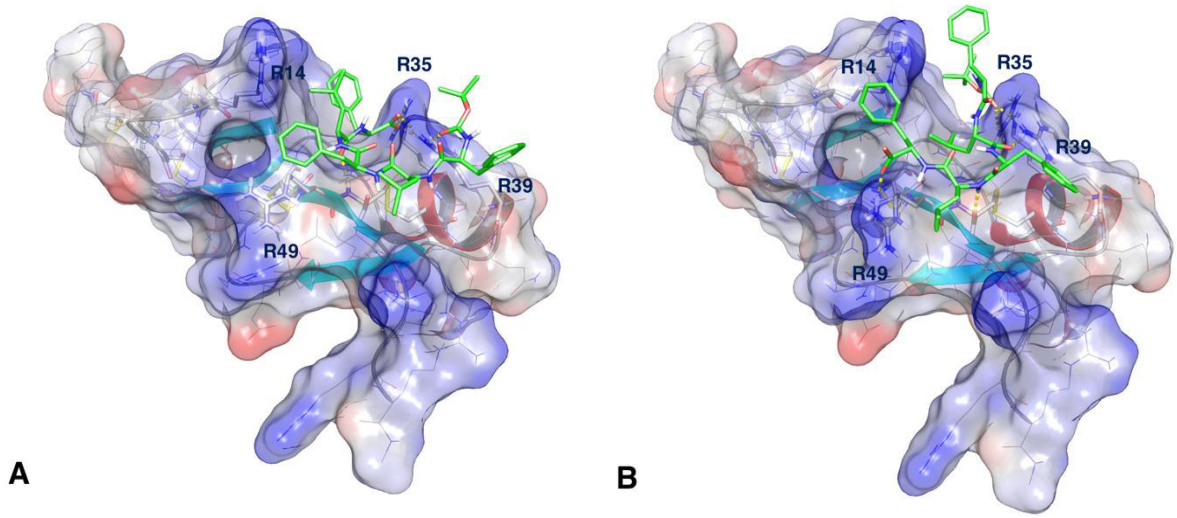


**Figure S2.** VEGF-HBD (grey carbon atoms) in complex with BOC2 (green carbon atoms) obtained by induced-fit docking. Panel A reports binding pose I (IFD score: 119.9 kcal $mol^{-1}$) while panel B reports binding pose II (IFD score: 119.7 kcal $mol^{-1}$). The molecular surface of VEGF-HBD is depicted with positively charged regions colored in blue, negatively regions in red and neutrals region in white.

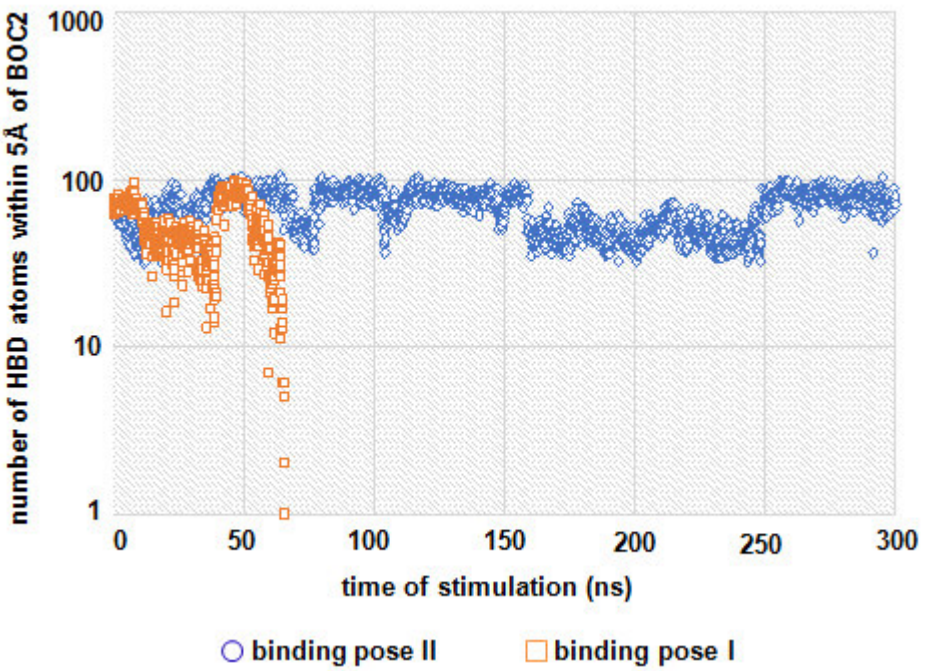


**Figure S3.** Time-series of the number of VEGF-HBD atoms (log scale) within a 5-Å radius from the structure of BOC2 recorded during the MD simulations. Orange dots refer to binding pose I, while blue dots refer to binding pose II simulation.

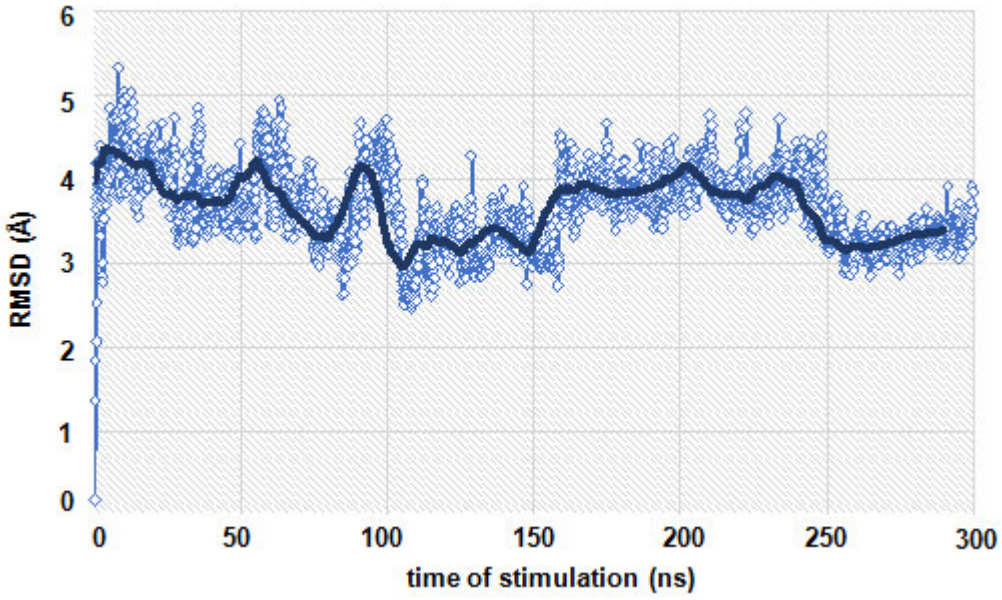


**Figure S4.** Time-series of the RMSD of the heavy atoms of BOC2 using the first snapshot of the MD simulation as reference structure. Blue dots report raw data, while the blue line reports the RMSD running average calculated over intervals of 10 ns.

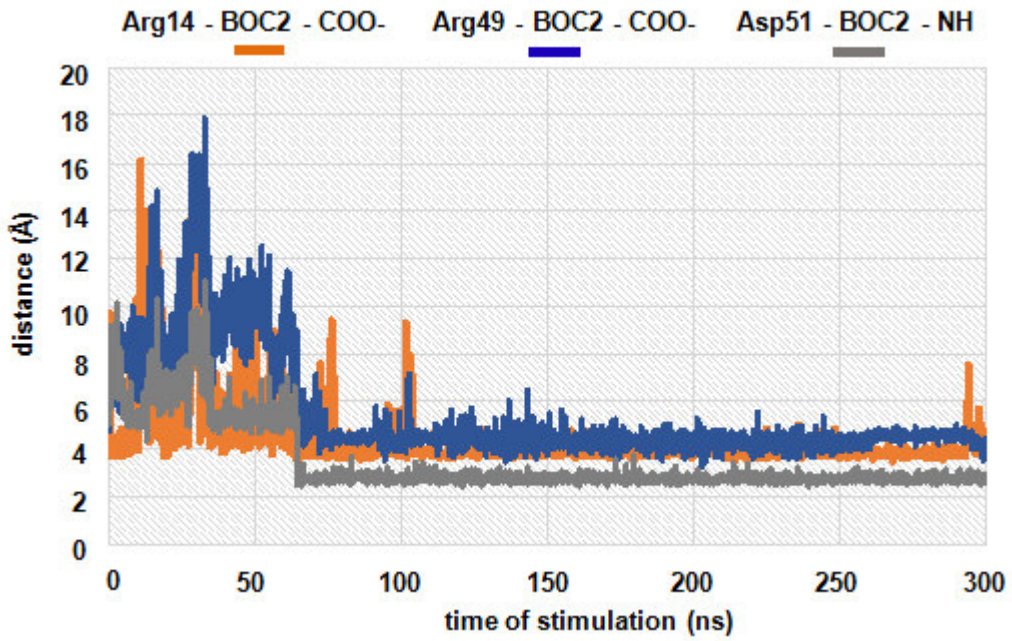


**Figure S5.** Time-series of key distances monitored during the MD simulation of VEGF-HBD in complex with BOC2 according with binding pose II. The orange line reports the distance between the carbonyl carbon of the BOC2 and carbonyl carbon of Arg14 guanidinium group, the blue line reports the distance between the carbonyl carbon of the BOC2 and carbonyl carbon of Arg49 guanidinium group, while the gray line reports the distance between the backbone nitrogen of Leu4 of BOC2 and Asp51 of VEGF-HBD.

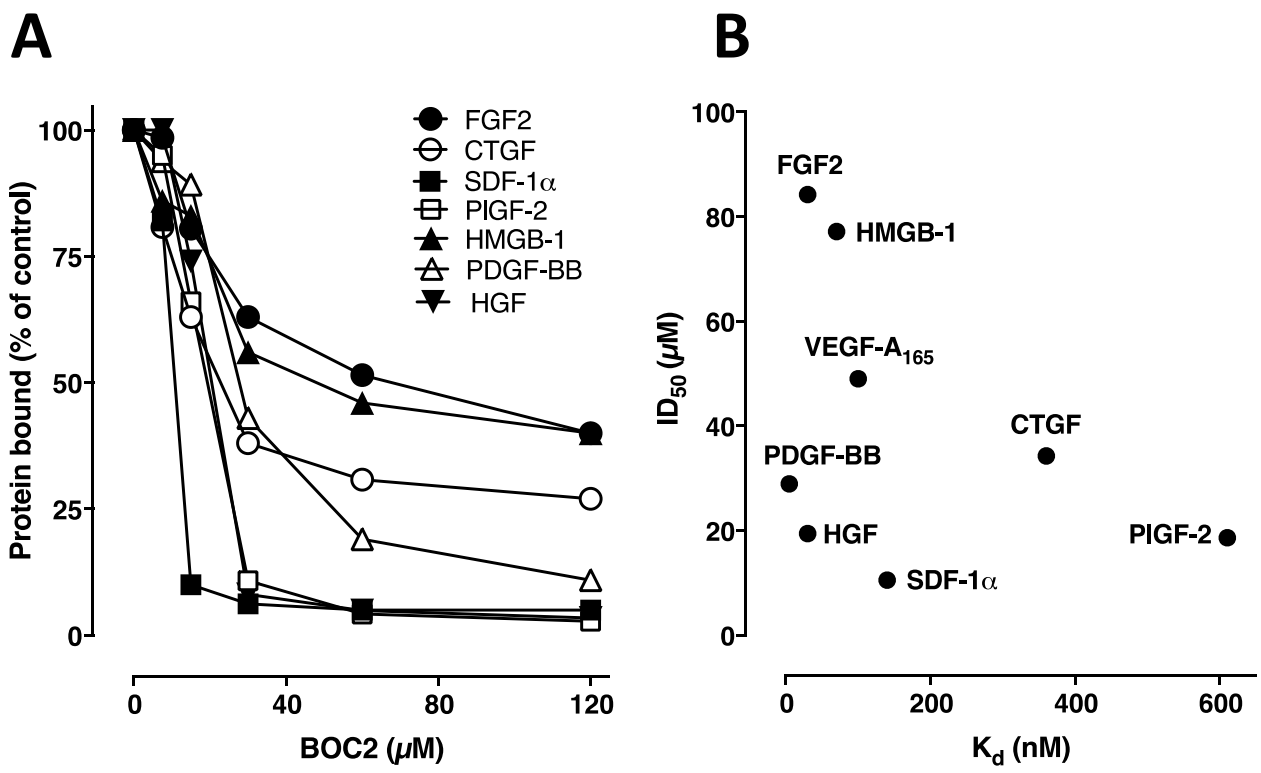


**Figure S6.** BOC2 inhibits the interaction of heparin-binding angiogenic growth factors with immobilized heparin. **A**) Fibroblast growth factor-2 (FGF2, ●), connective tissue growth factor (CTGF, ○), stromal cell-derived factor 1 (SDF-1, ■), placenta-derived growth factor-2 (PlGF-2, □), high mobility group box 1 (HMGB-1, ▲) platelet-derived growth factor-BB (PDGF-BB, △), and hepatocyte growth factor (HGF, ▼) were co-injected with increasing concentrations of BOC2 on heparin immobilized to a Biacore sensor chip. The response (in RU) was recorded at the end of injection and plotted as a function of BOC2 concentration. **B**) For each protein analyzed in panel A, its affinity for heparin interaction (expressed as SPR assessed $K_d$ value) was plotted *versus* the $ID_{50}$ value of BOC2-dependent inhibition of its binding to immobilized heparin.